ELSEVIER

Contents lists available at ScienceDirect

Earth and Planetary Science Letters

www.elsevier.com/locate/epsl



Stratigraphic control of landscape response to base-level fall, Young Womans Creek, Pennsylvania, USA



Roman A. DiBiase a,b,*, Alison R. Denn c, Paul R. Bierman c, Eric Kirby d, Nicole West e, Alan J. Hidy f

- ^a Department of Geosciences, Pennsylvania State University, University Park, PA, 16802, USA
- ^b Earth and Environmental Systems Institute, Pennsylvania State University, University Park, PA, 16802, USA
- ^c Department of Geology, University of Vermont, Burlington, VT, 05405, USA
- ^d College of Earth, Ocean, and Atmospheric Sciences, Oregon State University, Corvallis, OR, 97331, USA
- e Department of Earth and Atmospheric Sciences, Central Michigan University, Mount Pleasant, MI, 48859, USA
- f Center for Accelerator Mass Spectrometry, Lawrence Livermore National Laboratory, Livermore, CA, 94550, USA

ARTICLE INFO

Article history: Received 30 April 2018 Received in revised form 28 August 2018 Accepted 4 October 2018 Available online xxxx Editor: J.-P. Avouac

Keywords: beryllium-10 cosmogenic radionuclides erosion lithology Appalachian Plateau

ABSTRACT

Landscapes are thought to respond to changes in relative base level through the upstream propagation of a boundary that delineates relict from adjusting topography. However, spatially-variable rock strength can influence the topographic expression of such transient landscapes, especially in layered rocks, where strength variations can mask topographic signals expected due to changes in climate or tectonics. Here, we analyze the landscape response to base-level fall in Young Womans Creek, a 220 km² catchment on the Appalachian Plateau, USA underlain by gently folded Paleozoic sedimentary rocks. We measured in situ ¹⁰Be concentrations in stream sands from 17 nested watersheds, and used a spatially-distributed model of sediment and ¹⁰Be production to constrain a threefold increase in the rate of base-level fall propagating upstream from the catchment outlet. Using lidar topography and a nearby detailed stratigraphic section, we map the extent of continuous, blocky, resistant sandstone strata that act as a caprock overlying more easily erodible sandstones and siltstones. The caprock influences landscape response in two ways. First, it serves as a boundary between slowly eroding (11.5 m Myr⁻¹), lowsloping (3-5°) areas of relict topography and lower, steeper portions of the landscape adjusting to base-level fall. Second, hillslopes supported by the overlying caprock are armored with coarse sediment and are significantly steeper (20-30°) than hillslopes where the caprock has been eroded (10°), despite having similar erosion rates (36 mMyr⁻¹) and bedrock substrate. Our results illustrate how gently dipping, layered rocks engender complicated relationships between lithology, topography and erosion rate, highlighting the importance of understanding how rock material properties influence surface processes and landscape evolution.

© 2018 Elsevier B.V. All rights reserved.

1. Introduction

Transient landscapes, defined as landscapes still adjusting to spatiotemporal variations in climate, tectonics, or rock strength, provide opportunities for reconstructing the timing of past conditions important for understanding landscape evolution (Kirby and Whipple, 2012; Whittaker, 2012). Landscape adjustment is thought to be driven by the upstream propagation of a boundary that delineates a relict landscape, which retains information about past base-level conditions, and an adjusting landscape

that moves towards equilibrium with new boundary conditions (e.g., Crosby and Whipple, 2006). Field observations from studies of transient landscapes developed in homogeneous crystalline rocks show broadly similar behavior—an increase in the relative rate of base-level fall leads to steepened river channels, steepened hillslopes, and higher erosion rates downstream of knickpoints that separate relict from adjusting landscapes (e.g., Gallen et al., 2011; Hurst et al., 2012; DiBiase et al., 2015).

In landscapes with heterogeneous lithology, both the propagation and the topographic signatures of changes in base level are modulated by differences in rock strength (e.g., Cook et al., 2009). In particular, landscapes characterized by gently-dipping layered rocks can either mimic the morphology of transient landscapes (e.g., Miller, 1991) or lead to complicated feedbacks be-

^{*} Corresponding author.

E-mail address: rdibiase@psu.edu (R.A. DiBiase).

tween base level, erosion rate, and topography (Forte et al., 2016; Perne et al., 2017; Yanites et al., 2017). Consequently, inferring climate and tectonic histories of landscapes with layered rocks is not straightforward.

In situ-produced cosmogenic nuclides in stream sediment (e.g., ¹⁰Be in quartz) provide a way to measure catchment-averaged erosion rates over timescales necessary to evaluate the nature and degree of landscape disequilibrium. When applied to steadily eroding landscapes, the concentration of ¹⁰Be in stream sediments is inversely proportional to erosion rate (Brown et al., 1995; Granger et al., 1996). However, in transient landscapes the concentration of ¹⁰Be will reflect an average apparent erosion rate that depends on the spatially-variable erosion rates, isotope production rates, and quartz distribution in the landscape (Bierman and Steig, 1996). It is straightforward to assess, using stream sediment ¹⁰Be concentration, the erosion rates of landscapes above knickpoints, where erosion is typically uniform; it is more challenging to interpret the ¹⁰Be concentration samples downstream of knickpoints that reflect an unknown spatial variability in erosion rate (e.g., Willenbring et al., 2013).

In this paper, we use detrital *in situ*-produced ¹⁰Be concentrations in stream sands from nested catchments to determine the spatial variation of erosion rate in a transient landscape developed into gently-folded layered sedimentary rocks. We use lidar-derived topography and a detailed stratigraphic section to map the extent of a resistant caprock unit. Topographic and geologic maps aid in determining potential spatial patterns in erosion rate. Using a spatially-distributed ¹⁰Be flux model that traces the production and transport of *in situ* produced ¹⁰Be in quartz throughout the landscape, we compare modeled versus observed detrital sample ¹⁰Be concentrations to determine the best-fit spatial pattern of erosion rates. We then assess the topographic expression of this scenario and discuss the implications of caprock layers for modulating landscape response to base-level fall.

2. Study area

We focus our analysis on Young Womans Creek, a 220 km² tributary to the West Branch Susquehanna River draining the unglaciated Appalachian Plateau (Fig. 1). At long wavelengths (>10 km), the topography of the Appalachian Plateau reveals the structure of the underlying gently-folded Paleozoic strata (Fig. 1D). Higher topography is generally associated with synclines capped by resistant sandstone units, and breached anticlines tend to expose more erodible underlying units and form topographic lows (Hack, 1960). Modern climate varies minimally over the Appalachian Plateau due to the limited total relief across the region (600 m), and Young Womans Creek receives mean annual precipitation of approximately 1100 mm/yr (30-yr normals covering 1981–2010 (http://prism.oregonstate.edu)). Superimposed on this structural control of long-wavelength topography are a series of incised valleys that flow into the Susquehanna River. The boundary between low-relief, high-elevation topography and the steeper incised valleys is demarcated by river knickpoints argued to reflect a late Cenozoic increase in the rate of baselevel fall that has propagated upstream along the Susquehanna River and its tributaries (Miller et al., 2013). Detrital ¹⁰Be derived erosion rates determined from watersheds below these knickpoints range from 50-100 mMyr⁻¹, whereas erosion rates above knickpoints are 5-30 mMyr⁻¹ (Reuter, 2005; Miller et al., 2013). This large-scale landscape disequilibrium is challenging to reconcile with the long-term tectonic quiescence of the Appalachian Mountains (Hancock and Kirwan, 2007; Portenga et al., 2013; Gallen et al., 2013) and likely requires epeirogenic mechanisms of surface uplift, perhaps due to mantle-driven dynamic topography (e.g., Moucha et al., 2008; Miller et al., 2013).

At the hillslope scale (10s of m), the topography of the Appalachian Plateau reflects contrasts in rock strength resulting from alternating beds of layered, clastic sedimentary rocks. The rocks exposed at Young Womans Creek are primarily composed of Late Devonian to Mississippian sandstones and siltstones that include the Catskill, Huntley Mountain, and Burgoon Formations (Fig. 1B) (Berg et al., 1980). The Late Devonian Catskill Formation consists primarily of deltaic and lower fluvial-plain red beds of interbedded siltstones and fine-grained litharenites, the whole being approximately 40% sandstone. The litharenites are thickly-laminated to thin-bedded and display fissile-flaggy parting when naturally weathered (Colton and Luft, 1966; Berg and Edmunds, 1979). The Huntley Mountain Formation consists of a conformable, 200-mthick transition zone in which thin-bedded litharenites identical to those of the Catskill Formation transition upwards to thick-bedded, slabby, blocky sublitharenites of the overlying Burgoon Formation. The Huntley Mountain sandstones are arranged in approximately nine major fluvial fining-upwards sequences, the whole being approximately 85% sandstone (Fig. 1C). The Mississippian Burgoon Formation caps the sequence (Fig. 1C). It comprises predominately medium-grained, buff, strongly trough cross-bedded sublitharenites that exhibit slabby, rubbly, and blocky fragmentation, with less than 5% thin shales and coal. The base of the Burgoon Formation is commonly conglomeratic and locally lies on a regionally persistent red shale in the Huntley Mountain Formation called the Patton Shale (Colton and Luft, 1966; Berg and Edmunds, 1979). Thus, at Young Womans Creek there is a systematic trend up-section from weak to strong lithologies (assuming the thickness of sandstone beds and thus joint spacing (e.g., Gross, 1993) is reflective of rock strength), with the upper Huntley Mountain Formation and Burgoon Sandstone acting locally as a resistant caprock (Fig. 1C). The implication of this strength gradient on the expression of landscape adjustment to base-level fall is the focus of this study.

3. Methods

3.1. Detrital in situ-produced ¹⁰Be measurement in stream sands

We collected 17 nested fluvial sediment samples within the watershed of Young Womans Creek, from catchments ranging in size from 1-220 km² (Fig. 2A). Samples were collected in active channel deposits at least 20 m upstream of major tributary junctions and sieved in the field to the 250-850 um sand fraction. We purified quartz from these samples following Kohl and Nishiizumi (1992) and extracted ¹⁰Be following the methods of Corbett et al. (2016). ¹⁰Be/⁹Be ratios were measured at Lawrence Livermore National Laboratory in July 2017 and normalized to ICN standard 07KNSTD3110 with an assumed value of 2.85×10^{-12} (Nishiizumi et al., 2007). Our reported ¹⁰Be/⁹Be ratios (Table 1) were corrected using an average of n=3 process blanks $(6.43 \pm 2.00 \times 10^{-16})$. To calculate apparent erosion rates (i.e., assuming uniform watershed erosion), we determined the mean latitude, longitude, and elevation for each watershed and used this value and a rock density of 2.7 g cm⁻³ as inputs to the online CRONUS calculator, using wrapper script version 2.3, calc. 2.1, function 2, constants 2.3, muons 1, and the default calibration dataset (Balco et al., 2008). Following DiBiase (2018), we make no topographic shielding corrections for calculating apparent catchment-mean erosion rates.

3.2. Topographic analysis and mapping

We used a 3-m resolution lidar digital elevation model (http://www.docs.dcnr.pa.gov/topogeo/pamap/lidar/) to analyze hillslope and channel morphology and map the extent of caprock and caprock-supported topography in the Young Womans Creek catchment. We used the Pennsylvania statewide digital geologic map

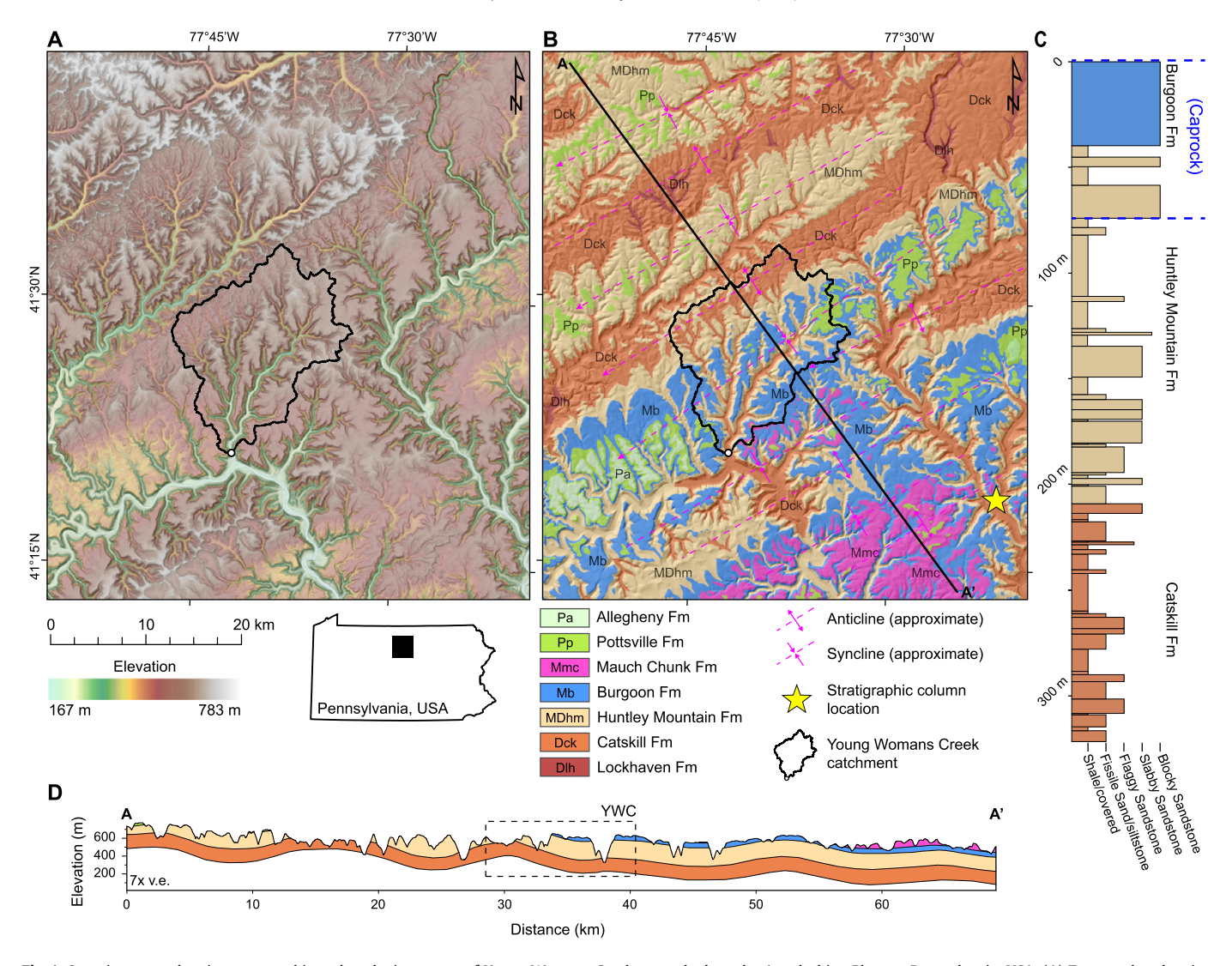


Fig. 1. Overview map showing topographic and geologic context of Young Womans Creek watershed on the Appalachian Plateau, Pennsylvania, USA. (A) Topography, showing incised valleys into low relief uplands. Black outline indicates extent of Young Womans Creek watershed. Shaded area in inset shows location of study area in Pennsylvania, USA. (B) Geology map (after Berg et al., 1980) showing approximate location of NE–SW trending folds that dictate large-scale topography (excluding incised valleys). (C) Generalized stratigraphic section at Huntley Mountain (star on panel (B); after Berg and Edmunds, 1979). Caprock at Young Womans Creek is defined as the Burgoon Formation sandstones and the upper blocky sandstones of the Huntley Mountain Formation. (D) Cross section A–A' showing regional structures and location of Young Womans Creek (YWC – dashed box).

(Berg et al., 1980) to infer geology at the regional scale (Fig. 1A) and used lidar hillshade and slope maps to refine mapping along a geologic cross section (Fig. 1C).

For Young Womans Creek, we generated hillshade and slope maps for visualization, and then used these to construct two geomorphic maps to derive spatial patterns in erosion rates: one map is characterized by topography alone (Fig. 2B), and the second is based on both topography and geology (Fig. 2C). Because relationships between mean slope and erosion rate are not valid at local (i.e., sub-hillslope) scales (e.g., Roering et al., 2007), we partitioned the landscape into zones with similar hillslope morphology, resulting in 75 "patches" ranging from <1 km² to 20 km². These patches were mapped using hillshade and slope base maps, and chosen to be large enough to incorporate multiple hillslopes such that the mean slope of each patch is comparable to the catchment-averaged slopes of sample watersheds and the mean hillslope angle from hillslope transport model predictions (e.g., Roering et al., 2007). We used the relationship between mean hillslope angle and apparent erosion rate determined for catchments in Young Womans Creek (Table 2) to define a linear least squares regression model for converting our map of patch mean slope (Fig. 2B) to a spatially-distributed map of erosion rates for input into our ¹⁰Be flux model (see Section 3.3). We also combined our data with previously published detrital ¹⁰Be data from the Appalachian Plateau extending to steeper slopes (Reuter, 2005; Miller et al., 2013) to constrain a nonlinear soil transport model for comparison.

For our combined topographic and geologic map, we aimed to map the extent of the resistant caprock consisting of the upper Huntley Mountain Formation and the Burgoon Formation, partitioning the remaining stratigraphically lower landscape into areas that retained the resistant caprock and areas where this caprock has been eroded from ridgelines. Initially, we used the Pennsylvania statewide digital geologic map (Berg et al., 1980) and a more detailed 1:24,000 scale map of the easternmost area of Young Womans Creek (Colton and Luft, 1966). We then refined our mapping of the caprock boundary by using a nearby (30 km SE) stratigraphic section of the upper Catskill Formation to Burgoon Formation (Berg and Edmunds, 1979) to identify the prominent base of uppermost blocky sandstone in the Huntley Mountain Formation (Star, Fig. 1B; Fig. 1C). The base of this marker bed was traced throughout the study area using the 3-m lidar slope map, and

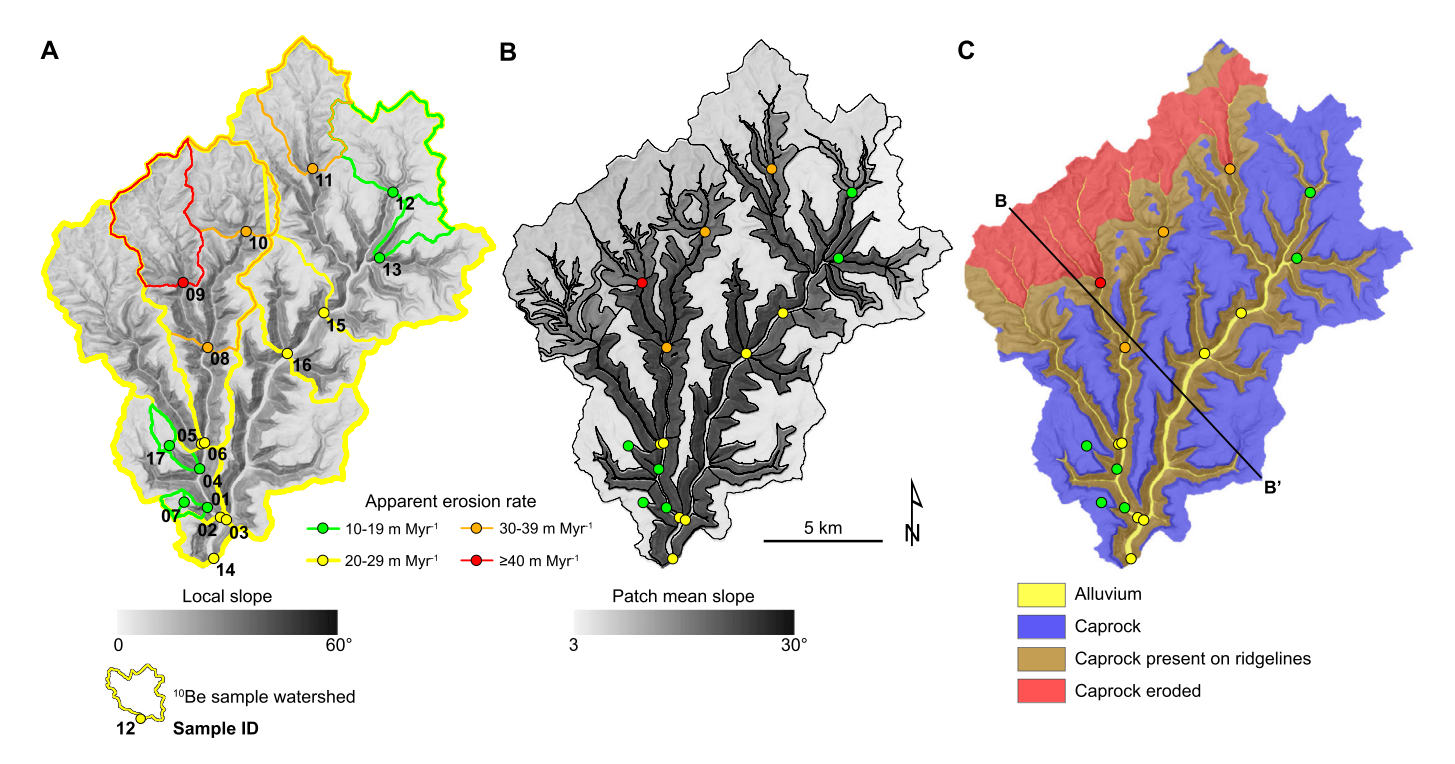


Fig. 2. Young Womans Creek watershed (location shown on Fig. 1). (A) Detrital 10 Be sample location map (circles = catchment outlet sample sites, outlines = watersheds) highlighting spatial pattern in apparent erosion rates. YW prefix in sample names omitted for clarity. (B) Map showing mean slope of n = 70 landscape "patches" (black outlines) that represent zones with similar hillslope morphology, which was used for input into the slope-dependent erosion model (Fig. 3, Fig. 5B). (C) Simplified geomorphic map highlighting extent of caprock (Burgoon Formation and upper Huntley Mountain Formation – Fig. 1C), topography where caprock is present on ridgelines, and areas where caprock has been completely eroded from ridgelines. B–B' indicates location of cross section shown in Fig. 7.

Table 1Laboratory preparation and accelerator mass spectrometry (AMS) analysis information for ¹⁰Be samples.

		=			=
Sample ID	Quartz mass (g)	⁹ Be added (µg)	Be cathode number ¹	Measured 10 Be/ 9 Be 2 (×10 $^{-15}$)	10 Be concentration (×10 ⁵ atoms g ⁻¹)
YW01	21.546	248.11	BE40780	322 ± 6	2.48 ± 0.05
YW02	22.889	247.87	BE40781	239 ± 8	1.73 ± 0.05
YW03	20.557	247.31	BE40782	247 ± 8	1.98 ± 0.06
YW04	22.102	248.11	BE40783	288 ± 6	2.16 ± 0.04
YW05	24.659	247.31	BE40785	227 ± 4	1.52 ± 0.03
YW06	15.725	247.84	BE40786	142 ± 4	1.50 ± 0.04
YW07	22.255	246.78	BE40787	400 ± 8	2.97 ± 0.06
YW08	17.547	247.99	BE40817	134 ± 3	1.27 ± 0.02
YW09	18.027	247.34	BE40818	112 ± 3	1.03 ± 0.03
YW10	14.233	247.64	BE40819	123 ± 4	1.43 ± 0.05
YW11	20.146	247.70	BE40820	159 ± 4	1.31 ± 0.03
YW12	22.390	247.40	BE40788	436 ± 10	3.22 ± 0.08
YW13	22.034	246.84	BE40790	516 ± 10	3.86 ± 0.07
YW14	20.833	245.78	BE40791	195 ± 4	1.54 ± 0.03
YW15	20.366	246.90	BE40821	233 ± 5	1.89 ± 0.04
YW16	20.038	246.52	BE40814	244 ± 5	2.00 ± 0.04
YW17	20.301	247.17	BE40823	495 ± 12	4.03 ± 0.10

¹ Identification for each sample within the database at the Center for Accelerator Mass Spectrometry at Lawrence Livermore National Laboratory, Livermore CA.

we defined as "caprock" everything above this stratigraphically (including the overlying Pottsville and Mauch Chunk Formations). We then used the extent of this caprock unit to map the remaining hillslopes as "caprock present on ridgelines" or "caprock eroded" if no caprock was present on ridgelines. Last, we mapped the extent of alluvial valley flats based on the slope and hillshade map.

Channel long profiles of Young Womans Creek and all tributaries with drainage area greater than 1 km² were extracted from the 3 m digital elevation model using the Topographic Analysis Kit for TopoToolbox (Schwanghart and Scherler, 2014;

Forte and Whipple, 2018). We smoothed profiles with a window of 500 m and constructed a map of the normalized channel steepness index, k_{SR} , as:

$$k_{\rm sn} = SA^{\theta_{\rm ref}},\tag{1}$$

where S is local channel gradient, A is upstream drainage area, and θ_{ref} is the reference concavity index, which we fix to 0.45 (Wobus et al., 2006). Knickpoints were mapped on channels with drainage area greater than 1 km² based on analysis of elevation long profiles and maps of normalized channel steepness.

² Normalized using ICN standard 07KNSTD3110 with a ratio of 2.85 \times 10⁻¹² (Nishiizumi et al., 2007). Reported errors are 1 σ AMS measurement uncertainties. Analyzed April 2016; data reduced using an average of n=3 process blanks (6.43 \pm 2.00 \times 10⁻¹⁶).

Table 2Sample catchment information.

Sample ID	Latitude	Longitude	Drainage area (km²)	Mean elevation (m)	Catchment mean slope (degrees)	Apparent erosion rate ¹ (m Myr ⁻¹)
YW01	41.3779	-77.7063	1.3	486	11.1	15.9 ± 0.3
YW02	41.3740	-77.6998	92.8	523	15.4	24.0 ± 0.8
YW03	41.3730	-77.6970	123.9	552	13.5	21.2 ± 0.7
YW04	41.3926	-77.7093	2.1	503	12.6	18.7 ± 0.4
YW05	41.4010	-77.7072	28.5	529	14.7	27.5 ± 0.6
YW06	41.4006	-77.7067	49.8	536	16.2	28.2 ± 0.8
YW07	41.3803	-77.7180	0.7	514	5.4	13.5 ± 0.3
YW08	41.4387	-77.7026	41.9	547	15.6	33.8 ± 0.7
YW09	41.4637	-77.7145	14.9	538	13.6	42 ± 1
YW10	41.4821	-77.6816	12.7	566	13.2	30 ± 1
YW11	41.5048	-77.6468	13.1	584	10.9	33.7 ± 0.8
YW12	41.4950	-77.6069	14.3	608	7.4	13.4 ± 0.3
YW13	41.4697	-77.6155	3.7	585	9.6	10.8 ± 0.2
YW14	41.3584	-77.7047	220.1	537	14.4	27.3 ± 0.5
YW15	41.4498	-77.6442	74.4	580	12.2	22.9 ± 0.6
YW16	41.4352	-77.6630	92.9	574	12.9	21.4 ± 0.4
YW17	41.4019	-77.7241	1.2	541	5.2	9.9 ± 0.3

¹ Apparent erosion rates (assuming uniform erosion rate) calculated using CRONUS calculator (Balco et al., 2008) wrapper script version 2.3, calc. 2.1, function 2, constants 2.3, muons 1, default calibration dataset, assuming density of 2.7 g cm⁻³.

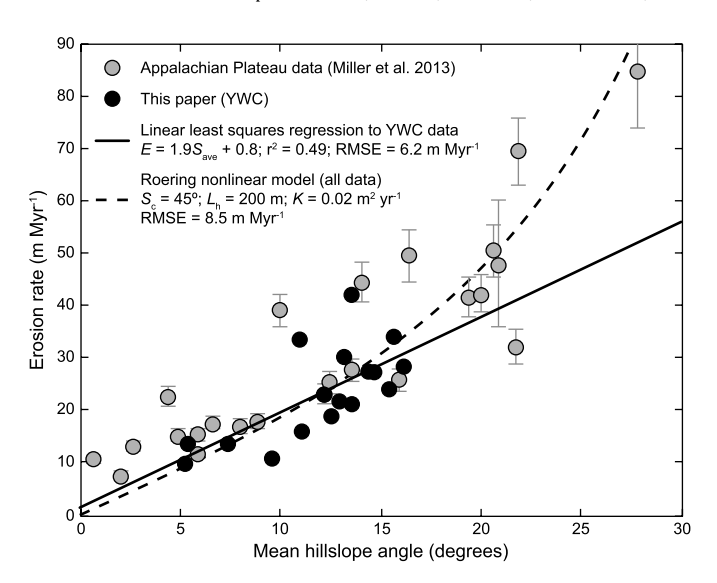


Fig. 3. Regional relationship between erosion rate determined from detrital 10 Be concentrations in stream sands and mean hillslope angle for the Appalachian Plateau. Solid line indicates linear regression through Young Womans Creek (YWC) data. Dashed line indicates a fit to all data using the hillslope-averaged form of the nonlinear soil transport model (Roering et al., 2007), assuming a critical slope, S_c , of 45° , mean hillslope length, L_h , of 200 m, and rock/soil density ratio of 2. Error bars for Appalachian Plateau data indicate 1σ analytical uncertainty. 1σ error bars for YWC data are smaller than the symbol size.

3.3. Spatially-distributed in situ-produced ¹⁰Be flux model

In order to use the ¹⁰Be concentrations of our 17 nested catchment samples to interpret spatial patterns in erosion rate, we used a spatially-distributed ¹⁰Be flux model to compare predicted and measured *in situ*-produced ¹⁰Be concentrations in quartz for four different spatially-distributed erosion scenarios. Our model combines and streamlines approaches from the existing erosion rate calculators CRONUS (Balco et al., 2008), CosmoCalc (Vermeesch, 2007), and CAIRN (Mudd et al., 2016) to calculate the local *in situ* ¹⁰Be flux out of the catchments assuming steady erosion and isotopic steady state at each pixel in the watershed of Young Womans Creek

Our model starts with a 10-m resolution lidar-derived digital elevation model and a 10-m resolution raster of spatially-distributed erosion rate. We follow the approach by Mudd et al. (2016)

and CosmoCalc v3.0 (http://www.ucl.ac.uk/~ucfbpve/cosmocalc/; Vermeesch, 2007) to simplify total spallogenic and muonogenic 10 Be production with depth as a sum of three exponential functions, and assume steady surface erosion to calculate the 10 Be concentration in quartz (atoms g^{-1}) at each pixel, $C_{^{10}\text{Re}}(i,j)$, as:

$$C_{10_{\text{Be}}}(i,j) = P_{SLHL} \sum_{m=1}^{3} \frac{S_m(i,j) F_m \Lambda_m}{E(i,j) + \lambda_{10_{\text{Be}}} \Lambda_m},$$
 (2)

where the subscripts i and j indicate raster pixel coordinates, P_{SLHL} is the surface production rate (atoms g^{-1} yr $^{-1}$) at sea level and high latitude; E(i,j) is a spatially-distributed erosion rate ($g\,cm^{-2}\,yr^{-1}$, assuming a rock density of 2.7 $g\,cm^{-3}$); $\lambda_{^{10}Be}$ is the decay constant for ^{10}Be (yr $^{-1}$); and $S_m(i,j)$, F_m , and Λ_m are scaling/shielding (dimensionless), pathway partitioning (dimensionless), and attenuation length ($g\,cm^{-2}$) parameters for the three-exponential approximation of spallogenic and muonogenic ^{10}Be production (Mudd et al., 2016). We assume values for P_{SLHL} (4.3 atoms $g^{-1}\,yr^{-1}$), $\Lambda_{1,2,3}$ (160, 1500, 4320 $g\,cm^{-2}$), and $F_{1,2,3}$ (0.9887, 0.0027, 0.0086) following Mudd et al. (2016) and Cosmo-Calc v3.0 (http://www.ucl.ac.uk/~ucfbpve/cosmocalc/; Vermeesch, 2007), and assume $\lambda_{^{10}Be} = 5 \times 10^{-7}\,yr^{-1}$ (Chmeleff et al., 2010). Consequently, there are slight (<5%) differences in the total ^{10}Be production rates between the approximation in Equation (2) and the CRONUS calculator (Mudd et al., 2016) that we assume are negligible when comparing erosion rates determined from the two methods.

The scaling/shielding parameter $S_m(i,j)$ incorporates both production rate scaling and topographic shielding and varies as a function of ¹⁰Be production pathway. We follow the approach of Vermeesch (2007) to calculate a virtual attenuation length, $\Lambda_{\nu}(i,j)$, in units of g cm⁻² according to:

$$S_{tot}(i,j) = \sum_{m=1}^{3} S_m(i,j) F_m,$$
 (3a)

$$S_m(i,j) = e^{\frac{-\Lambda_V(i,j)}{\Lambda_m}},\tag{3b}$$

where $S_{tot}(i, j)$ is the total scaling/shielding, defined as:

$$S_{total}(i,j) = S_t(i,j)S_p(i,j). \tag{4}$$

 $S_t(i, j)$ is the topographic shielding parameter, which we assume to be unity at each pixel. Full treatment of topographic shielding at

the catchment scale is presently computationally impractical, but calculations based on simplified catchment geometry indicate that the influence of increasing vertical attenuation length with slope offsets reductions in surface production rate due to skyline shielding such that no spatially-distributed correction factor is needed for local slopes less than 30° as observed in Young Womans Creek (DiBiase, 2018). We calculate the production rate scaling factor, $S_p(i,j)$, using the Lal/Stone constant production rate model applied using the latitude and longitude of each pixel (Lal, 1991; Stone, 2000). While in general Equation (3) must be solved iteratively, for efficiency we approximate $\Lambda_v(i,j)$ for Young Womans Creek as:

$$\Lambda_{\nu}(i,j) = -161.5 \ln S_{total}(i,j), \tag{5}$$

which is accurate to 0.1% for the range $1 < S_{total}(i,j) < 2$ and encompasses the values of all pixels in the Young Womans Creek catchment.

To determine the *in situ*-produced ¹⁰Be flux per unit area (atoms cm⁻² yr⁻¹) from each pixel in the watershed, $q_{^{10}\text{Be}}(i, j)$, we scale the concentration at each pixel by the erosion rate, E(i, j), and dimensionless quartz mass fraction, $f_{atz}(i, j)$:

$$q_{10_{\text{Re}}}(i,j) = C_{10_{\text{Re}}}(i,j)E(i,j)f_{atz}(i,j). \tag{6}$$

We determined the spatial variation in quartz content by assuming that the areas mapped as caprock contained 85% quartz and the non-caprock units contained 75% quartz in the grain sizes analyzed (Berg and Edmunds, 1979).

To calculate the modeled 10 Be concentration (atoms g^{-1}) of a well-mixed sample of stream sands, we normalized the total *in situ*-produced 10 Be flux by the total quartz flux out of the upstream contributing area according to:

$$Model_{{}^{10}\text{Be}}(n) = \frac{1}{A_n} \sum_{A} \frac{q_{{}^{10}\text{Be}}(i,j)}{E(i,j)f_{qtz}(i,j)},\tag{7}$$

where $Model_{^{10}Be}(n)$ is the modeled sample concentration (atoms g^{-1}) for a catchment with areal extent A_n . We assess the fit of modeled and observed sample ^{10}Be concentrations using the root mean square error, RMSE, defined as:

$$RMSE = \sqrt{\frac{1}{N} \sum_{n=1}^{N} \left(Model_{10}_{Be}(n) - Observed_{10}_{Be}(n) \right)^2}, \tag{8}$$

where $Observed_{^{10}Be}(n)$ corresponds to the measured sample ^{10}Be concentrations from the N=17 samples.

As a result of streamlining the calculation of simulated ¹⁰Be concentrations in sample watersheds, we take a systematic grid approach to exploring parameter space for one, two, and three parameter erosion models based on the combined geologic and topographic map (Fig. 2C) and for comparison run two models based on the patch mean slope map (Fig. 2B) converted to erosion rate using the linear least squares regression and nonlinear soil transport models shown in Fig. 3.

Using the combined geologic and topographic map (Fig. 2C), we tested all combinations (Fig. 4) of the caprock erosion rate in 0.5 m Myr⁻¹ increments from 9–15 m Myr⁻¹ (Blue area, Fig. 2C); the caprock-protected hillslope erosion rate in 1 m Myr⁻¹ increments from 20–45 m Myr⁻¹ (Brown area, Fig. 2C); and the eroded caprock hillslope erosion rate in 1 m Myr⁻¹ increments from 30–50 m Myr⁻¹ (Red area, Fig. 2C). We assumed the areas mapped as alluvium eroded at the same rate as the caprock-protected hillslope erosion rate; this region comprises only a minor component of the total ¹⁰Be flux in all models (<3% of catchment surface area concentrated in areas of low ¹⁰Be production rate – yellow area, Fig. 2C).

4. Results

4.1. Spatial patterns of apparent erosion rates

Interpreting the detrital ^{10}Be concentrations as coming from uniformly eroding catchments provides a visualization of the spatial pattern in apparent erosion rates, which range from 9.9 ± 0.3 to 42 ± 1 mMyr $^{-1}$ (Table 2). Apparent erosion rates are highest for catchments draining the northwestern tributaries where the caprock has been eroded $(30\pm1$ to 42 ± 1 mMyr $^{-1})$ and are lowest for catchments that exclusively drain the caprock units $(9.9\pm0.3$ to 13.5 ± 0.3 mMyr $^{-1}$). Larger, nested catchments have intermediate apparent erosion rates that smoothly integrate the variability found in lower-order tributary samples (Fig. 2A).

There is considerable scatter in the relationship between catchment-mean hillslope angle and apparent erosion rate (Fig. 3), in agreement with similar data from elsewhere on the Appalachian Plateau (Reuter, 2005; Miller et al., 2013). Notably, the catchments with the highest erosion rates (YW08, YW09, YW10, YW11) are not correlated with the steepest hillslopes in the watershed (Fig. 2B), suggesting a lithologic control on landscape form. Nonetheless, we used the empirical relationship between mean slope and erosion rate for Young Womans Creek and nearby data (Fig. 3) to build a spatially-distributed map of erosion rates as one input to our ¹⁰Be flux model.

4.2. Constraints on spatial patterns in erosion rate from the in situ-produced ¹⁰Be flux model

For the simplest case of uniform erosion rate (Fig. 5A), detrital ^{10}Be concentrations for the best-fit case ($E=20~\text{mMyr}^{-1}$) are predicted to fall within a narrow range ($\pm5\%$) that reflects the limited variation in elevation (200–700 m) and latitude (41.35–41.55°N) throughout Young Womans Creek. These variations are further dampened by averaging across watersheds. In contrast, measured ^{10}Be concentrations vary over a factor of four (1–4 \times 10^5 atoms g $^{-1}$), suggesting the integrated cosmic-ray exposure and thus erosion rates do in fact vary throughout the catchment.

Assuming erosion rate scales linearly with mean hillslope angle following Fig. 2B and Fig. 3, modeled 10 Be concentrations vary from 1.4–4.0 \times 10⁵ atoms g⁻¹ and show a stronger correlation with measured 10 Be concentrations (black symbols, Fig. 5B). However, this model over-predicts by 20–70% the concentrations of the four samples with the lowest measured 10 Be concentration (YW08–YW11), all of which come from the northwest area of the catchment where the caprock has been eroded (Fig. 2A). Using a nonlinear soil transport model (dashed line, Fig. 3) results in a poorer overall fit to the data (gray symbols, Fig. 5B).

The best-fit three-parameter model, based on the combined topographic and geologic mapping (Fig. 2C), indicates a caprock erosion rate of $11.5 \,\mathrm{m\,Myr^{-1}}$; a caprock-protected hillslope erosion rate of $34 \,\mathrm{m\,Myr^{-1}}$, and an eroded caprock hillslope erosion rate of $40 \,\mathrm{m\,Myr^{-1}}$ (Fig. 5C; blue star, Fig. 4). Partitioning of the landscape into regions based on topographic position of the caprock provides a stronger fit to the measured data than either the uniform erosion rate case (Fig. 4A) or the slope-dependent erosion rate case (Fig. 5B), as determined by the RMSE. Notably, the error is greatly reduced ($\pm 10\%$) for the four samples draining the hillslopes where the caprock has been eroded. Additionally, the 10 Be concentrations for the two samples with the greatest absolute error (YW13 and YW17) are only underestimated by 10-20%.

In addition to finding the best-fit model using a three-parameter fit, we also evaluated a simpler, two-parameter fit, where only the caprock erosion rate and non-caprock erosion rate was varied (1:1 lines, Fig. 4). The best-fit model for the two-parameter case indicates a caprock erosion rate of $11.5~{\rm m\,Myr^{-1}}$ and a non-caprock

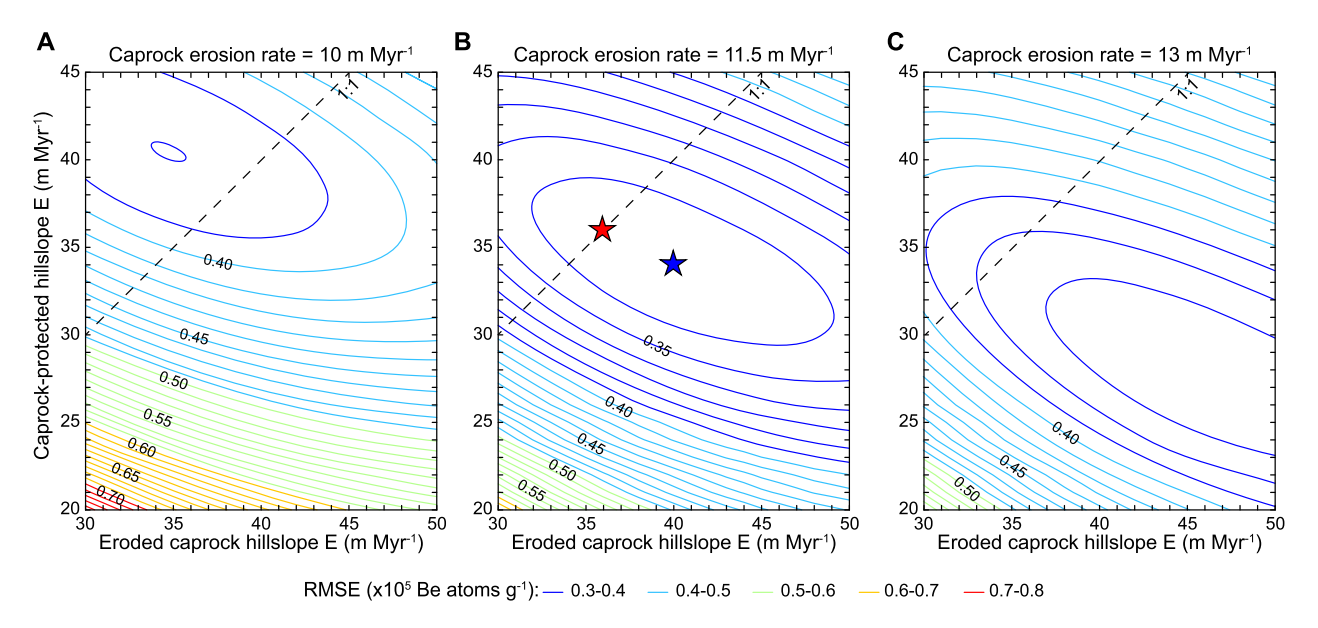


Fig. 4. Spatially-distributed *in situ*-produced ¹⁰Be flux model results for 3 parameter erosion model, with contours of root mean squared error (RMSE) between measured and predicted concentrations for caprock erosion rate equal to: (A) 10 mMyr⁻¹; (B) 11.5 mMyr⁻¹; and (C) 13 mMyr⁻¹. Blue star in (B) indicates global minimum for 3 parameter model (Fig. 5C). Red star in (B) indicates best-fit case with uniform erosion for areas below caprock (2 parameter model: Fig. 5D). Dashed line indicates 1:1 line between caprock-protected hillslope E and eroded caprock hillslope E (i.e., 2 parameter model space). (For interpretation of the colors in the figure(s), the reader is referred to the web version of this article.)

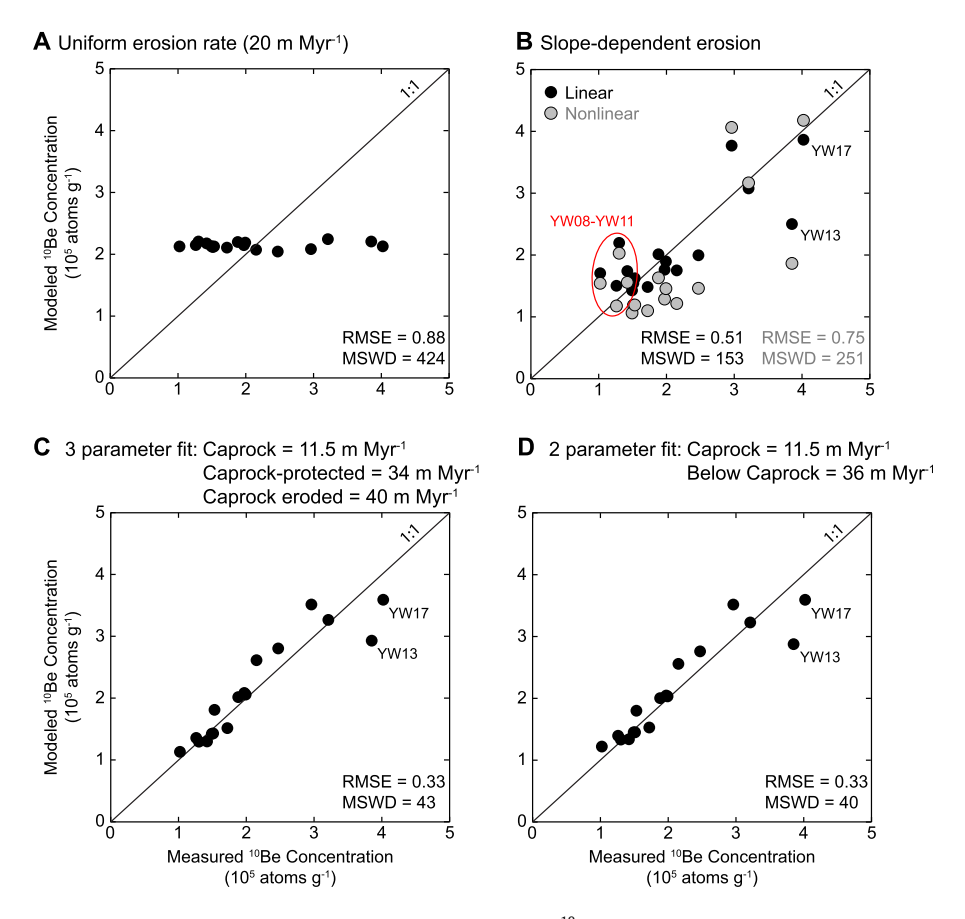


Fig. 5. Results from spatially-variable erosion rate model comparing predicted versus observed 10 Be concentrations in nested catchments of Young Womans Creek. (A) Null case, assuming uniform erosion rate (20 m Myr $^{-1}$ is best fit scenario). (B) Slope-dependent erosion case, showing over prediction of concentrations in areas of catchment where the caprock has been eroded (Red circle, samples YW08–YW11 – Fig. 2C). Black symbols indicate linear fit in Fig. 3, and gray symbols indicate nonlinear fit in Fig. 3. (C) Best-fit case for 3 parameter model (see Fig. 2C for mapping). (D) Best fit case for 2 parameter model (grouping all areas below caprock together). Error bars (1 σ analytical uncertainty) are smaller than the symbol size.

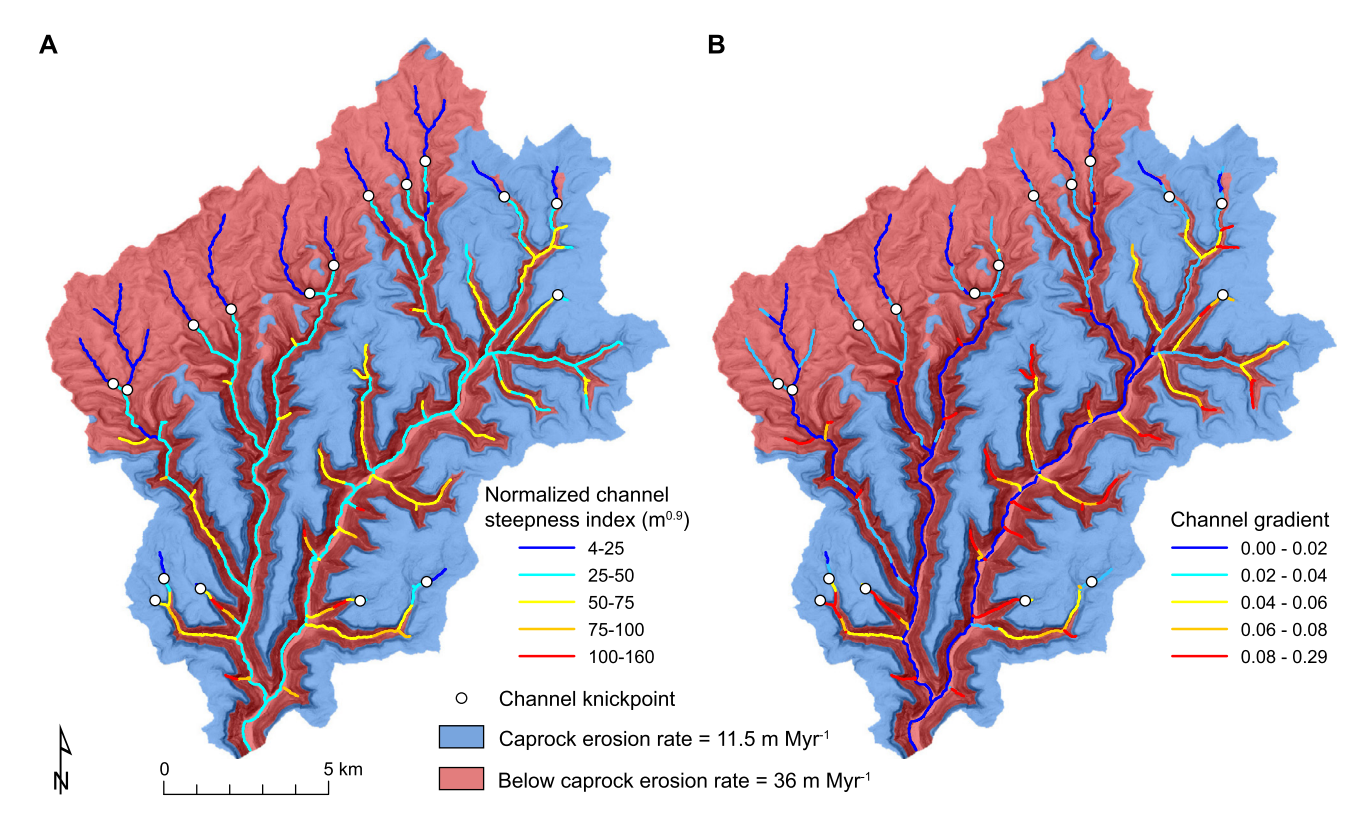


Fig. 6. Map of channel network in Young Womans Creek with drainage area greater than 1 km² colorized by: (A) normalized channel steepness index; and (B) local channel gradient. Knickpoints are indicated by white circles. Base map is colorized by the spatial pattern in erosion rate for the best-fit 2-parameter model (Fig. 5D).

erosion rate of 36 mMyr $^{-1}$ (Fig. 5D). As the two-parameter model fit is nearly indistinguishable from the three-parameter model fit (RMSE $=0.33\times10^5$ atoms g^{-1}), we favor this simpler interpretation

For each of the cases in Fig. 5, we also calculated the mean square weighted deviation, MSWD, to evaluate the degree to which the misfit of our model can be explained by analytical measurement uncertainty:

$$MSWD = \frac{1}{17 - m} \sum_{n=1}^{17} \frac{(Model_{10Be}(n) - Observed_{10Be}(n))^2}{\sigma(n)^2}, \quad (9)$$

where $\sigma(n)$ is the standard deviation of each 10 Be measurement and m is the number of fitted parameters. For the two-parameter best fit case, MSWD = 40, suggesting poor model performance for the precision of the measured data. However, we only account for the analytical uncertainty in our measured 10 Be concentrations ($1\sigma=2-3\%$); inclusion of even a modest 5% additional error (e.g., due to uncertainty in production rate scaling, shielding, or spatial variations in quartz content) results in MSWD = 3.

4.3. Connection between erosion rate and topography

The normalized channel steepness of Young Womans Creek and its tributaries ranges from 4–160 m^{0.9}, corresponding to channel gradients ranging from 0.005–0.29 (Fig. 6) and showing a similar spatial pattern to that of mean hillslope angle, which ranges from 3–30° (Fig. 2B). Where the caprock is preserved on overlying hillslopes (Fig. 2C), there exists a sharp break in topography that delineates a low-sloping, slowly eroding landscape from a steeper, more rapidly eroding landscape (Fig. 2B; Fig. 6). However, in areas where the caprock is no longer preserved on ridgelines, both hillslope and channel steepness are subdued, despite high erosion rates (Fig. 6; Fig. 7).

5. Discussion

5.1. Deconvolution of spatially-distributed erosion rates from nested detrital $^{10}\mathrm{Be}$ samples

Typically, detrital ¹⁰Be-derived erosion rates from nested catchments are deconvolved using simple mixing calculations for two basins (e.g., Granger et al., 1996). Here, we showed how incorporation of a dense network of nested samples can be used to robustly assess spatial patterns in erosion rate in a transient land-scape, where interpretations based on apparent erosion rates may be misleading (Fig. 2A). Although we used geologic context to constrain potential patterns in erosion rate, our approach does not require any *a priori* assumptions of topographic or rock strength controls on erosion rate. Thus, it is possible to test hypotheses relating to potentially complicated feedbacks between baselevel fall, rock strength, and erosion rate (e.g., Forte et al., 2016; Perne et al., 2017; Yanites et al., 2017).

Implicit in our approach is the assumption that apparent erosion rates inferred from detrital ¹⁰Be concentrations are insensitive to catchment size. This assumption is likely valid for the Young Womans Creek study area, which is characterized by soil-mantled hillslopes and slow erosion rates. However, in steep landscapes subject to landsliding, episodic sediment delivery could violate assumptions of isotopic steady state in small catchments (e.g., Niemi et al., 2005) and in very large catchments, sediment storage could alter isotope concentrations over time (Bierman and Steig, 1996).

5.2. Implications for regional patterns of erosion rate and base-level fall on the Susquehanna River

Despite geologic complexity, Young Womans Creek is most simply interpreted as a catchment responding to an approximately threefold increase in the rate of base-level fall (11.5 $\rm m\,Myr^{-1}$ to 36 $\rm m\,Myr^{-1}$). This signal has propagated upstream and the caprock

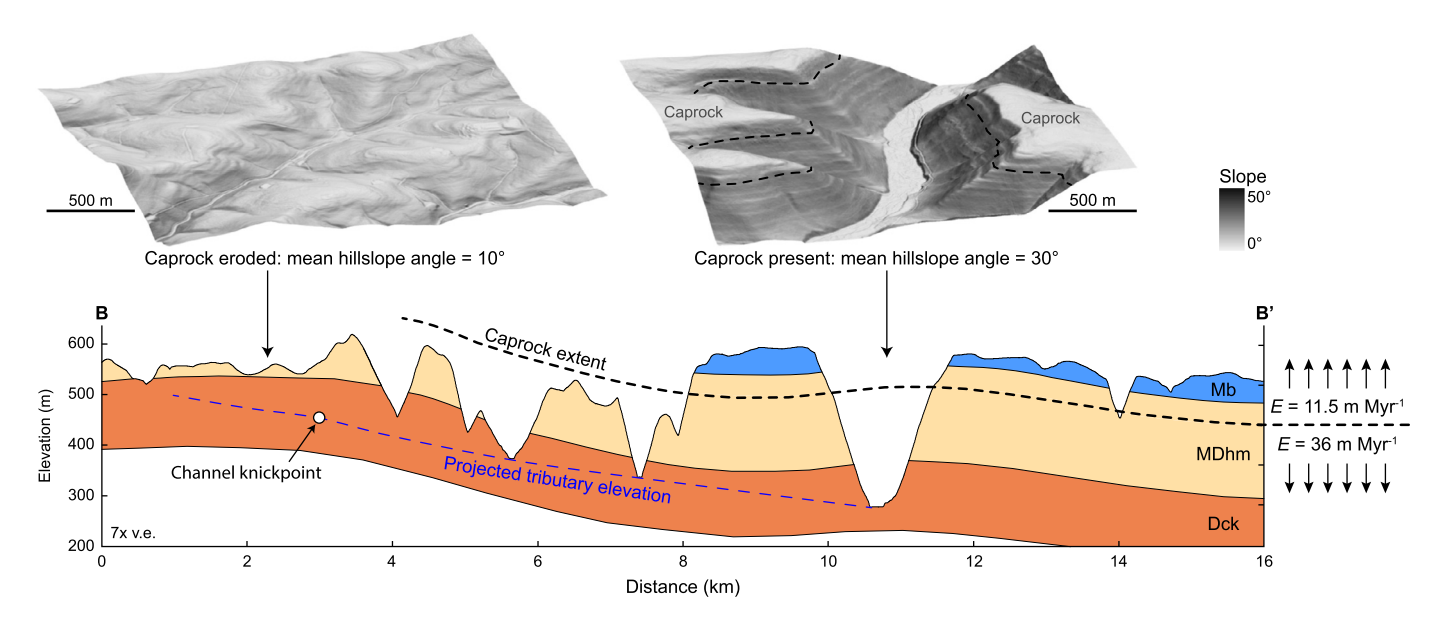


Fig. 7. Cross section B-B' across Young Womans Creek watershed (see Fig. 2C for location), indicating contrasting hillslope morphology in areas where the caprock has been eroded versus where the caprock is still present along ridgelines. Dashed blue line indicates the projected elevation of tributaries on western side of Young Womans Creek and maximum structural depth of erosion, with tributary channel knickpoint indicated by the white circle. Dashed black line indicates the location and extent of the caprock contact, which has been projected onto cross section based on exposure on adjacent ridges along-strike. Geologic units are labeled as in Fig. 1.

contact defines the extent of a slowly eroding, relict landscape (Fig. 6). At its outlet, Young Womans Creek has incised approximately 200 m below the caprock contact. Based on a difference in erosion rate of 24.5 mMyr⁻¹ between the relict and adjusting portions of the landscape, we estimate incision into the Appalachian Plateau at Young Womans Creek began ca. 8 Ma. Both the contrast in erosion rates and the timing of incision are consistent with regional interpretations of late Cenozoic base-level fall (Pazzaglia and Brandon, 1996; Gallen et al., 2013; Miller et al., 2013; Brantley et al., 2016).

Although we lack constraints on the progression of landscape adjustment during the past 8 Ma, the coincidence of the caprock and the boundary between relict and adjusting landscapes in Young Womans Creek (Fig. 2) highlights a structural and lithologic control on landscape adjustment to base-level fall (e.g., Cook et al., 2009). In particular, the absence of both a caprock and slowly eroding terrain in the northwestern portion of Young Womans Creek indicates that the caprock serves to slow knickpoint retreat and preserve relict topography (e.g., DiBiase et al., 2015). Additionally, knickpoints on northwestern tributaries of Young Womans Creek are not associated with a contrast in erosion rate (Fig. 6), indicating a lithologic control on their morphology and location. Further work is needed to constrain the mechanisms by which the caprock limits knickpoint propagation (e.g., via coarse sediment delivery, more resistant bedrock, or change in incision process), and which lithologic factors lead to the presence of low-steepness channels with high erosion rates (Fig. 6).

Landscape evolution models simulating base-level fall in gently folded layered rocks predict complicated patterns in erosion rate that emerge due to transient breaching of alternating hard and soft layers by river networks (Forte et al., 2016; Perne et al., 2017; Yanites et al., 2017). Although we see no evidence for such complications at Young Womans Creek, it is not clear whether such signals are expected or resolvable, particularly because contrasts in bedrock erodibility may be masked by non-local effects of coarse sediment delivered from resistant units armoring channels (e.g., Johnson et al., 2009; Thaler and Covington, 2016).

5.3. Caprock control on hillslope morphology

Based on our ¹⁰Be flux model, we interpret a bimodal distribution of erosion rates for areas above and below the basal caprock contact (Fig. 2C; Fig. 6). Thus, it might be expected that hillslope form reveals a similar contrast. Instead, we find that hillslopes where the caprock has been preserved on ridges are systematically steeper (mean slope = 20–30°; Fig. 2B) than hillslopes where the caprock has been eroded (mean slope = 10°; Fig. 2B), despite having the same erosion rate and underlying bedrock stratigraphy (Fig. 7). We hypothesize that this contrast in hillslope erodibility emerges due to armoring of soft strata with coarse blocks derived from resistant caprock sandstones (Fig. 8) (e.g., Granger et al., 2001; Glade et al., 2017).

A caprock control on hillslope morphology is common in landscapes characterized by layered rocks (Howard and Selby, 2009), and can lead to complicated relationships between topography, lithology, and erosion rate. For example, in the Buffalo River Basin of the Ozark Plateau, USA, Thaler and Covington (2016) showed how boulders derived from a resistant sandstone caprock led to steeper streams in underlying weaker strata where the caprock was still preserved on ridgelines. Observations in the Buffalo River Basin of the morphology of hillslopes underlain by slope-forming limestones show a similar pattern. Where capped by resistant sandstone strata, weaker limestone slopes are steep (20-30°) and planar; where the resistant caprock has been eroded, the weaker limestone slopes are less steep (<10°) and convex. Although in the Buffalo River Basin there are fewer constraints on erosion rate than in Young Womans Creek, the landscape morphology shows a clear signature of caprock control that may be responsible for the large amount of scatter observed in relationships between mean hillslope angle and erosion rate, even for similar rocks (Beeson et al., 2017). Such structural and lithologic controls on hillslope and channel erodibility can make straightforward interpretations of spatiotemporal variations in climate, tectonics, or divide migration problematic (e.g., Whipple et al., 2017).







Fig. 8. Contrasting soil texture of hillslopes with: (A) caprock eroded; and (B) caprock present. Hillslopes in panels A and B are underlain by similar bedrock stratigraphy and are eroding at similar rates. However, a coarse armor of sandstone blocks derived from upslope caprock units (C) leads to steeper hillslopes where the caprock is present.

6. Conclusions

This study highlights the complexities that can emerge in landscapes with layered rocks due to feedbacks among lithology, topography, and erosion rate. We showed how spatial patterns in erosion rate can be deconvolved in transient landscapes using a nested sampling strategy for in situ-produced ¹⁰Be in stream sediment paired with a spatially-distributed in situ-produced ¹⁰Be flux model. Based on constraints from lidar-derived geologic mapping at Young Womans Creek, we found that measured 10 Be concentrations are most simply explained by a two-parameter model with erosion rates of 11.5 mMyr⁻¹ on low relief topography above a distinctive sandstone caprock and erosion rates of 36 mMyr⁻¹ below this level. This contrast in erosion rates implies that Young Womans Creek is responding to a threefold increase in baselevel fall that began ca. 8 Ma, in agreement with regional estimates in the Susquehanna River Basin (Miller et al., 2013). Because the boundary of relict and adjusting landscapes is pinned at the

caprock, we interpret that the presence of the caprock has prolonged the timescale of landscape adjustment. Below this caprock unit, hillslopes eroding at the same rate and underlain by the same rocks have strongly contrasting morphology, depending on whether the overlying caprock is preserved on adjacent ridgelines or not. Field observations indicate that the resulting contrast in downslope soil transport efficiency is a consequence of coarse sediment derived from the caprock that armors underlying hillslopes. Thus, even a relatively simple case of increased base-level fall in gently folded rocks can lead to a complex morphologic response that is difficult to interpret without a dense, nested, detrital ¹⁰Be sampling strategy.

Acknowledgements

This project was funded by the National Science Foundation Critical Zone Observatories program (grant NSF-EAR 13-31726 to S.L. Brantley). Cosmogenic data in this publication were generated with the support of NSF-EAR 1735676 to P.R. Bierman. This work was performed in part under the auspices of the U.S. Department of Energy by Lawrence Livermore National Laboratory under Contract DE-AC52-07NA27344. This is LLNL-JRNL-750365. We thank Rudy Slingerland for insightful discussions about the regional stratigraphy of the Appalachian Plateau. Comments from two anonymous reviewers helped improve the manuscript.

Appendix A. Supplementary material

Supplementary material related to this article can be found online at https://doi.org/10.1016/j.epsl.2018.10.005.

References

Balco, G., Stone, J.O., Lifton, N.A., Dunai, T.J., 2008. A complete and easily accessible means of calculating surface exposure ages or erosion rates from ¹⁰Be and ²⁶Al measurements. Quat. Geochronol. 3, 174–195. https://doi.org/10.1016/j.quageo. 2007.12.001.

Beeson, H.W., McCoy, S.W., Keen-Zebert, A., 2017. Geometric disequilibrium of river basins produces long-lived transient landscapes. Earth Planet. Sci. Lett. 475, 34–43. https://doi.org/10.1016/j.epsl.2017.07.010.

Berg, T., Edmunds, W., Geyer, A., Glover, A., Hoskins, D., MacLachlan, D., Root, S., Sevon, W., Socolow, A., 1980. Geologic Map of Pennsylvania. Pennsylvania Geological Survey. 4th ser. Map 1, 3.

Berg, T.M., Edmunds, W.E., 1979. The Huntley Mountain Formation: Catskill-to-Burgoon transition in north-central Pennsylvania. Commonwealth of Pennsylvania Department of Environmental Resources, Bureau of Topographic and Geologic Survey. Information Circular 83.

Bierman, P., Steig, E.J., 1996. Estimating rates of denudation using cosmogenic isotope abundances in sediment. Earth Surf. Process. Landf. 21, 125–139. https://doi.org/10.1002/(SICI)1096-9837(199602)21:2<125::AID-ESP511>3.0.CO;2-8.

Brantley, S.L., DiBiase, R.A., Russo, T.A., Shi, Y., Lin, H., Davis, K.J., Kaye, M., Hill, L., Kaye, J., Eissenstat, D.M., Hoagland, B., Dere, A.L., Neal, A.L., Brubaker, K.M., Arthur, D.K., 2016. Designing a suite of measurements to understand the critical zone. Earth Surf. Dyn. 4, 211–235. https://doi.org/10.5194/esurf-4-211-2016.

Brown, E.T., Stallard, R.F., Larsen, M.C., Raisbeck, G.M., Yiou, F., 1995. Denudation rates determined from the accumulation of *in situ*-produced ¹⁰Be in the Luquillo experimental forest, Puerto Rico. Earth Planet. Sci. Lett. 129, 193–202. https://doi.org/10.1016/0012-821X(94)00249-X.

Chmeleff, J., von Blanckenburg, F., Kossert, K., Jakob, D., 2010. Determination of the ¹⁰Be half-life by multicollector ICP-MS and liquid scintillation counting. Nucl. Instrum. Meth. B. 268, 192–199. https://doi.org/10.1016/j.nimb.2009.09.012.

Colton, G.W., Luft, S.J., 1966. Bedrock Geology of the Slate Run Quadrangle, Clinton, Lycoming, and Potter Counties, Pennsylvania. Pennsylvania Bureau of Topographic and Geological Survey. PR 167, scale 1:24,000.

Cook, K.L., Whipple, K.X., Heimsath, A.M., Hanks, T.C., 2009. Rapid incision of the Colorado River in Glen Canyon—insights from channel profiles, local incision rates, and modeling of lithologic controls. Earth Surf. Process. Landf. 34, 994–1010. https://doi.org/10.1002/esp.1790.

Corbett, L.B., Bierman, P.R., Rood, D.H., 2016. An approach for optimizing in situ cosmogenic ¹⁰Be sample preparation. Quat. Geochronol. 33, 24–34. https://doi.org/10.1016/j.quageo.2016.02.001.

Crosby, B.T., Whipple, K.X., 2006. Knickpoint initiation and distribution within fluvial networks: 236 waterfalls in the Waipaoa River, North Island, New Zealand. Geomorphology 82, 16–38. https://doi.org/10.1016/j.geomorph.2005.08.023.

- DiBiase, R.A., 2018. Short communication: increasing vertical attenuation length of cosmogenic nuclide production on steep slopes negates topographic shielding corrections for catchment erosion rates. Earth Surf. Dyn. Discuss. https://doi.org/ 10.5194/esurf-2018-48.
- DiBiase, R.A., Whipple, K.X., Lamb, M.P., Heimsath, A.M., 2015. The role of waterfalls and knickzones in controlling the style and pace of landscape adjustment in the western San Gabriel Mountains, California. Geol. Soc. Am. Bull. 127, 539–559. https://doi.org/10.1130/B31113.1.
- Forte, A.M., Yanites, B.J., Whipple, K.X., 2016. Complexities of landscape evolution during incision through layered stratigraphy with contrasts in rock strength. Earth Surf. Process. Landf. 41, 1736–1757. https://doi.org/10.1002/esp.3947.
- Forte, A.M., Whipple, K.X., 2018. Short communication: the topographic analysis kit (TAK) for TopoToolbox. Earth Surf. Dyn. Discuss. https://doi.org/10.5194/esurf-2018-57.
- Gallen, S.F., Wegmann, K.W., Bohnenstieh, D.R., 2013. Miocene rejuvenation of to-pographic relief in the southern Appalachians. GSA Today 23, 4–10. https://doi.org/10.1130/GSATG163A.1.
- Gallen, S.F., Wegmann, K.W., Frankel, K.L., Hughes, S., Lewis, R.Q., Lyons, N., Paris, P., Ross, K., Bauer, J.B., Witt, A.C., 2011. Hillslope response to knickpoint migration in the Southern Appalachians: implications for the evolution of post-orogenic landscapes. Earth Surf. Process. Landf. 36, 1254–1267. https://doi.org/10.1002/ esp.2150.
- Glade, R.C., Anderson, R.S., Tucker, G.E., 2017. Block-controlled hillslope form and persistence of topography in rocky landscapes. Geology 45, 311–314. https:// doi.org/10.1130/G38665.1.
- Granger, D.E., Kirchner, J.W., Finkel, R., 1996. Spatially averaged long-term erosion rates measured from *in situ*-produced cosmogenic nuclides in alluvial sediment. J. Geol. 104, 249–257. https://doi.org/10.1086/629823.
- Granger, D.E., Riebe, C.S., Kirchner, J.W., Finkel, R.C., 2001. Modulation of erosion on steep granitic slopes by boulder armoring, as revealed by cosmogenic ²⁶Al and ¹⁰Be. Earth Planet. Sci. Lett. 186, 269–281. https://doi.org/10.1016/S0012-821X/01)00236-9.
- Gross, M.R., 1993. The origin and spacing of cross joints: examples from the Monterey Formation, Santa Barbara Coastline, California. J. Struct. Geol. 15, 737–751. https://doi.org/10.1016/0191-8141(93)90059-J.
- Hack, J.T., 1960. Interpretation of erosional topography in humid temperate regions. Am. J. Sci. 258-A, 80-97.
- Hancock, G., Kirwan, M., 2007. Summit erosion rates deduced from ¹⁰Be: implications for relief production in the central Appalachians. Geology 35, 89–92. https://doi.org/10.1130/G23147A.1.
- Howard, A.D., Selby, M.J., 2009. Rock slopes. In: Parsons, J., Abrahams, A.D. (Eds.), Geomorphology of Desert Environments. Springer, Netherlands, pp. 189–232.
- Hurst, M.D., Mudd, S.M., Walcott, R., Attal, M., Yoo, K., 2012. Using hilltop curvature to derive the spatial distribution of erosion rates. J. Geophys. Res. 117, F02017. https://doi.org/10.1029/2011/F002057.
- Johnson, J.P., Whipple, K.X., Sklar, L.S., Hanks, T.C., 2009. Transport slopes, sediment cover, and bedrock channel incision in the Henry Mountains, Utah. J. Geophys. Res., Earth Surf. 114, F02014. https://doi.org/10.1029/2007JF000862.
- Kirby, E., Whipple, K.X., 2012. Expression of active tectonics in erosional landscapes. J. Struct. Geol. 44, 54–75. https://doi.org/10.1016/j.jsg.2012.07.009.
- Kohl, C.P., Nishiizumi, K., 1992. Chemical isolation of quartz for measurement of insitu-produced cosmogenic nuclides. Geochim. Cosmochim. Acta 56, 3583–3587. https://doi.org/10.1016/0016-7037(92)90401-4.
- Lal, D., 1991. Cosmic ray labeling of erosion surfaces: in situ nuclide production rates and erosion models. Earth Planet. Sci. Lett. 104, 424–439. https://doi.org/10.1016/0012-821X(91)90220-C.
- Miller, J.R., 1991. The influence of bedrock lithology on knickpoint development and channel-bed degradation along downcutting streams in south-central Indiana. J. Geol. 99, 591–605. https://doi.org/10.1086/629519.
- Miller, S.R., Sak, P.B., Kirby, E., Bierman, P.R., 2013. Neogene rejuvenation of central Appalachian topography: evidence for differential rock uplift from stream pro-

- files and erosion rates. Earth Planet. Sci. Lett. 369–370, 1–12. https://doi.org/10. 1016/j.epsl.2013.04.007.
- Moucha, R., Forte, A.M., Mitrovica, J.X., Rowley, D.B., Quéré, S., Simmons, N.A., Grand, S.P., 2008. Dynamic topography and long-term sea-level variations: there is no such thing as a stable continental platform. Earth Planet. Sci. Lett. 271, 101–108. https://doi.org/10.1016/j.epsl.2008.03.056.
- Mudd, S.M., Harel, M.A., Hurst, M.D., Grieve, S.W.D., Marrero, S.M., 2016. The CAIRN method: automated, reproducible calculation of catchment-averaged denudation rates from cosmogenic nuclide concentrations. Earth Surf. Dyn. 4, 655–674. https://doi.org/10.5194/esurf-4-655-2016.
- Niemi, N.A., Oskin, M., Burbank, D.W., Heimsath, A.M., Gabet, E.J., 2005. Effects of bedrock landslides on cosmogenically determined erosion rates. Earth Planet. Sci. Lett. 237, 480–498. https://doi.org/10.1016/j.epsl.2005.07.009.
- Nishiizumi, K., Imamura, M., Caffee, M.W., Southon, J.R., Finkel, R.C., McAninch, J., 2007. Absolute calibration of ¹⁰Be AMS standards. Nucl. Instrum. Meth. B 258, 403–413. https://doi.org/10.1016/j.nimb.2007.01.297.
- Pazzaglia, F.J., Brandon, M.T., 1996. Macrogeomorphic evolution of the post-Triassic Appalachian mountains determined by deconvolution of the offshore basin sedimentary record. Basin Res. 8, 255–278. https://doi.org/10.1046/j.1365-2117. 1996.00274.x.
- Perne, M., Covington, M.D., Thaler, E.A., Myre, J.M., 2017. Steady state, erosional continuity, and the topography of landscapes developed in layered rocks. Earth Surf. Dyn. 5, 85–100. https://doi.org/10.5194/esurf-5-85-2017.
- Portenga, E.W., Bierman, P.R., Rizzo, D.M., Rood, D.H., 2013. Low rates of bedrock outcrop erosion in the central Appalachian Mountains inferred from in situ ¹⁰Be. Geol. Soc. Am. Bull. 125, 201–215. https://doi.org/10.1130/B30559.1.
- Reuter, J.M., 2005. Erosion Rates and Patterns Inferred from Cosmogenic ¹⁰Be in the Susquehanna River Basin. MS thesis. University of Vermont, Burlington, Vermont. 160 p.
- Roering, J.J., Perron, J.T., Kirchner, J.W., 2007. Functional relationships between denudation and hillslope form and relief. Earth Planet. Sci. Lett. 264, 245–258. https://doi.org/10.1016/j.epsl.2007.09.035.
- Schwanghart, W., Scherler, D., 2014. Short communication: TopoToolbox 2 MATLAB-based software for topographic analysis and modeling in Earth surface sciences. Earth Surf. Dyn. 2, 1–7. https://doi.org/10.5194/esurf-2-1-2014.
- Stone, J.O., 2000. Air pressure and cosmogenic isotope production. J. Geophys. Res., Solid Earth 105, 23753–23759. https://doi.org/10.1029/2000JB900181.
- Thaler, E.A., Covington, M.D., 2016. The influence of sandstone caprock material on bedrock channel steepness within a tectonically passive setting: Buffalo National River Basin, Arkansas, USA. J. Geophys. Res., Earth Surf. 121, 1635–1650. https:// doi.org/10.1002/2015JF003771.
- Vermeesch, P., 2007. CosmoCalc: an Excel add-in for cosmogenic nuclide calculations. Geochem. Geophys. Geosyst. 8, Q08003. https://doi.org/10.1029/2006GC001530.
- Whipple, K.X., Forte, A.M., DiBiase, R.A., Gasparini, N.M., Ouimet, W.B., 2017. Timescales of landscape response to divide migration and drainage capture: implications for the role of divide mobility in landscape evolution. J. Geophys. Res., Earth Surf. 122, 248–273. https://doi.org/10.1002/2016JF003973.
- Whittaker, A.C., 2012. How do landscapes record tectonics and climate? Lithosphere 4, 160–164. https://doi.org/10.1130/RF.L003.1.
- Willenbring, J.K., Gasparini, N.M., Crosby, B.T., Brocard, G.Y., 2013. What does a mean mean? The temporal evolution of detrital cosmogenic denudation rates in a transient landscape. Geology 41, 1215–1218. https://doi.org/10.1130/G34746.1.
- Wobus, C., Whipple, K.X., Kirby, E., Snyder, N., Johnson, J., Spyropolou, K., Crosby, B., Sheehan, D., 2006. Tectonics from topography: procedures, promise, and pitfalls. Spec. Pap., Geol. Soc. Am. 398, 55–74. https://doi.org/10.1130/2006.2398(04).
- Yanites, B.J., Becker, J.K., Madritsch, H., Schnellmann, M., Ehlers, T.A., 2017. Lithologic effects on landscape response to base level changes: a modeling study in the context of the Eastern Jura Mountains, Switzerland. J. Geophys. Res., Earth Surf. 122, 2196–2222. https://doi.org/10.1002/2016JF004101.